PERGAMON

International Journal of Solids and Structures 38 (2001) 2893–2919

INTERNATIONAL JOURNAL OF SOLIDS and STRUCTURES

www.elsevier.com/locate/ijsolstr

Compensation for thermal deformation of a paraboloid shell using distributed structural actuation

Dongyao Tan

Department of Aeronautics, Imperial College of Science, Technology and Medicine, Prince Consort Road, London SW7 2BY, UK

Received 12 February 1999; in revised form 5 May 2000

Abstract

A simulation procedure is described in this paper for investigating the deformation control in advanced plate and shell structures which have the so-called adaptive capabilities using smart materials. The procedure is an iterative one which involves sensing and actuating processes. The former measures structural responses and determines how the actuators act whilst the latter realizes the actuation and dictates the new structural deformation state. The structural modelling used in the procedure is completely based on the classical plate and shell theory, and the constitutive relationship involved has a general type for laminated composites which integrates the structural and smart materials and facilitates that smart materials can be embedded in or bonded on the structure. A co-located sensing and actuating scheme based on strain measurement is employed. This procedure is tested with an example of thermal deformation control for a plate first and then applied to the compensation for thermal deformation of a paraboloid shell of revolution which models an antenna. © 2001 Published by Elsevier Science Ltd.

Keywords: Smart structures; Doubly-curved shells; Composites; Distributed structural actuation; Thermal deformation

1. Introduction

The new interdisciplinary study of smart materials and structures emerged about a decade and half years ago. It was first an outcome of a desire for high-performance aircraft structures with smart skins and large flexible space structures with integrated actuators to control their deformations and suppress their vibrations. Then it has widely penetrated into other engineering branches, like automotive engineering, civil engineering, maritime engineering and bio-mechanical engineering. Increasingly more and more technical books and journal papers are discussing this topic and has resulted in even more researchers getting involved in it. Gandhi and Thompson (1992) talked generally about the smart materials and structures and especially their future perspectives; Banks et al. (1996) and Preumont (1997) focused on the vibration control of structures integrated with piezoelectric actuators; Culshaw (1996) introduced more about the optical sensing besides other electrostrictive and magnetostrictive sensors and actuators. In the simulation analysis of smart structures, two methodologies have been used in modelling establishment. The first

E-mail address: bcd.tan@tinyonline.co.uk (D. Tan).

0020-7683/01/$ - see front matter © 2001 Published by Elsevier Science Ltd.
PII: S0020-7683(00)00211-0

methodology separates the smart materials or actuators from the structures and uses conventional structural elements, like the bar and beam elements, to model the structures alone and add the mass, damping and stiffness properties of the smart materials or actuators on the structural models directly. This methodology has been used in vibration suppression for large flexible space truss structures and seismic space frame structures (see e.g. Adeli and Saleh (1998) and the references therein). The second methodology integrates smart materials and structural materials into the finite element modelling. Therefore, the elements constructed in this way will have variable material properties which will result in the variable damping and stiffness properties for the elements. Plate-type of such elements has been investigated by numerous researchers (see e.g. Crawly and his co-workers (1987, 1991), Ha et al. (1992), Lin and his co-workers (1993, 1996), Chandrashekhara and Agarwal (1993), Chattopadhyay and Seeley (1997)) and applied to the deformation control and vibration suppression for plates. Other general topics in smart materials and structures can be found in a more complete bibliography survey given by Mackerle (1998).

This paper proposes a procedure to construct an element for a shell of revolution in which smart materials may be present. The smart materials are assumed to be layered type which can be bonded on or embedded in a shell structure to provide sensing and induced strain actuating functions. The overall material properties of a shell structure are modelled as that of general laminated composites. Therefore, the stress and moment resultants corresponding to the thermal strain and the induced actuation strain of the smart materials can be obtained straightforwardly using the constitutive relationship for general laminated composites. Fig. 1 shows a typical lay-up of the laminated composites of interest with layered smart materials.

Under the assumption that a shell structure of interest is thin, the classical shell theory is used to describe its deformation. Rayleigh–Ritz approach is then employed to deduce the element stiffness matrix and nodal force vector of which the latter may contain the actuation from the smart materials. The structural strain responses, which are readily measurable in real implementation, are calculated in the present simulation analysis and taken as the sensing quantities. A control algorithm based on a co-located sensing and actuating scheme is adopted in which the action of an actuator depends only on the sensing measurement of a sensor located in the same place. To test the procedure, the controlled deflections of a composite beam for which an analytical solution exists and a cantilevered laminated composite plate with distributed G-1195 piezoelectric ceramics bonded on the surfaces of the plate for which experimental results are available from Crawly and de Luis (1987) and an actuator composite plate exposed to elevated environment for which a finite element simulation was carried out by Ha et al. (1992) are investigated. Then, this procedure is

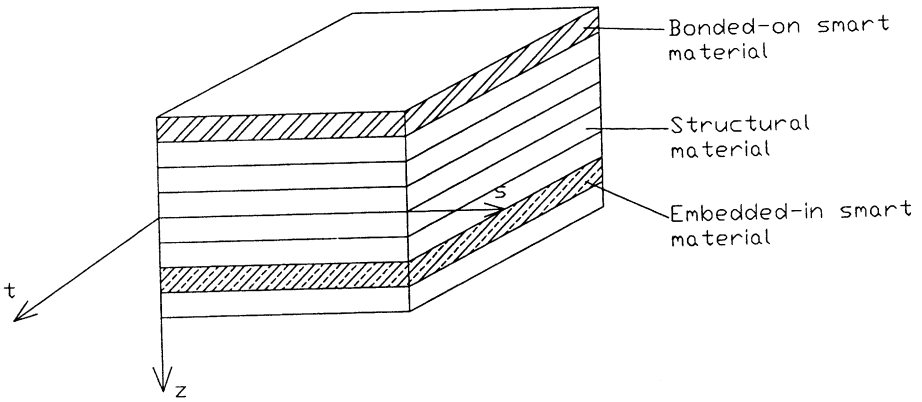

Fig. 1. A typical lay-up of laminated composites with layered smart materials.

applied to analyze the shape control problem of a thermally deformed paraboloid shell of revolution (modelling an antenna) and generate numerical simulations about its deformation control using different control schemes with respect to various thermal environments to which it is exposed.

2. Governing equations of the thermal deformation control problems using induced strain actuation

Finite element method is used in this paper to simulate the thermal deformation control process for plates and shells with distributed structural actuation. Therefore, the governing equations are established with the use of energy variational principles. Rayleigh–Ritz approach based on the minimum strain potential energy is employed here. So, to obtain the governing equation, the expression for the strain potential energy is needed first. In the particular problem discussed in this paper, it has the following rather simple form,

$$U = \frac{1}{2}\int_V \sigma^{\mathrm{T}}(\varepsilon - \varepsilon_{\mathrm{T}} - \varepsilon_{\mathrm{A}})\,\mathrm{d}V, \tag{1}$$

where $\varepsilon - \varepsilon_{\mathrm{T}} - \varepsilon_{\mathrm{A}}$ is the elastic strain in which ε is the total strain which relates to structural displacement field, ε_{T} the thermal strain and ε_{A} the induced actuation strain. In Eq. (1), σ is the stress state which depends on the elastic strain through the constitutive relationship of materials, i.e.

$$\sigma = \mathbf{C}(\varepsilon - \varepsilon_{\mathrm{T}} - \varepsilon_{\mathrm{A}}), \tag{2}$$

where $\mathbf{C}$ is material modulus matrix.

For plate and shell structures, the strain potential energy can also be expressed in terms of membrane strains and bending curvatures after the through thickness integration has been carried out in Eq. (1), e.g.

$$U = \frac{1}{2}\int_\Omega \mathbf{e}^{\mathrm{T}}\left(\mathbf{L}\mathbf{e} - 2\mathbf{F}^{(\mathrm{T})} - 2\mathbf{F}^{(\mathrm{A})}\right)\mathrm{d}\Omega + U_0, \tag{3}$$

where U_0 is a constant strain potential energy term due to the thermal and induced actuation strains, Ω is structural mid-surface area, vector $\mathbf{e}$ consists of membrane strains and bending curvatures which relates to stress resultants through matrix $\mathbf{L}$, $\mathbf{F}^{(\mathrm{T})}$ and $\mathbf{F}^{(\mathrm{A})}$ which are stress resultants from the thermal and induced actuation strains, respectively. Their detailed forms will be given in later sections based on their counterparts in each element.

In finite element approach, the displacement field is interpolated from those at element nodes by shape functions. Therefore, membrane strains and bending curvatures can finally be expressed with those displacement values according to the specific kinematics adopted in the classical plate and shell theory used here, i.e.

$$\mathbf{e} = \mathbf{\Phi}\mathbf{D}, \tag{4}$$

where $\mathbf{D}$ is the unknown displacement vector which is composed of those at element nodes whilst $\mathbf{\Phi}$ is the so-called strain matrix.

Substituting Eq. (4) into Eq. (3) and applying variations on the result, we obtain the governing equations in weak form,

$$\delta U = \delta\mathbf{D}^{\mathrm{T}}\left(\left[\int_\Omega \mathbf{\Phi}^{\mathrm{T}}\mathbf{L}\mathbf{\Phi}\,\mathrm{d}\Omega\right]\mathbf{D} - \int_\Omega \mathbf{\Phi}^{\mathrm{T}}\mathbf{F}^{(\mathrm{T})}\,\mathrm{d}\Omega - \int_\Omega \mathbf{\Phi}^{\mathrm{T}}\mathbf{F}^{(\mathrm{A})}\,\mathrm{d}\Omega\right) = \mathbf{0}, \tag{5}$$

i.e.

$$\mathbf{K}\mathbf{D} - \mathbf{f}^{(\mathrm{T})} - \mathbf{f}^{(\mathrm{A})} = \mathbf{0}, \tag{6}$$

where $\mathbf{K} = \int_\Omega \mathbf{\Phi}^T \mathbf{L} \mathbf{\Phi} \, d\Omega$ is the structural stiffness matrix, $\mathbf{f}^{(T)} = \int_\Omega \mathbf{\Phi}^T \mathbf{F}^{(T)} \, d\Omega$ and $\mathbf{f}^{(A)} = \int_\Omega \mathbf{\Phi}^T \mathbf{F}^{(A)} \, d\Omega$ are equivalent nodal forces corresponding to thermal and induced actuation strains, respectively. It is well known that in the real implementation of finite element approach, the variational principles are used at element level, and structural stiffness matrix and nodal force vectors are assembled from those of elements in a standard way. So, in the following sections, we concentrate on element construction.

3. Displacement representation of an element as a piece of shell of revolution

3.1. Geometry description of an element

Fig. 2 shows a basic element of a shell of revolution which may, in general, be a laminate (Fig. 1) having arbitrary lay-up of a number of layers of fibre-reinforced composite or smart material. In the element, the natural co-ordinates are used. For a shell of revolution, this natural co-ordinate system is orthogonal and happens to be the lines of curvature.

Under the assumption that the shells are thin, the classical thin shell theory (TST) is employed which uses three displacement-type quantities indicated in Fig. 2, namely u, v and w, the translational displacements at the middle surface in the s, t and z directions, respectively, to characterize the shell behaviour. In the present approach, the physical displacements are only specified at some locations on the several so-called reference meridians (four reference meridians are shown in Fig. 1). The displacements elsewhere in an element are interpolated from them. On the reference meridians, the spline interpolation is used which facilitates the required displacement continuity along the meridians to be maintained and the kinematic boundary condition at two ends of the shells to be satisfied. Between the reference meridians, the polynomial interpolation is used which observes the condition that no additional physical displacements are needed other than those specified on the reference meridians.

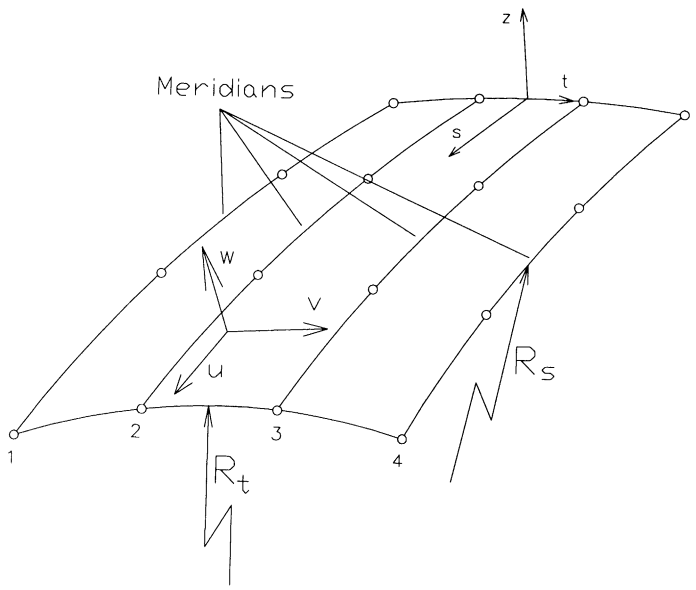

Fig. 2. An element.

3.2. Displacement representation along a meridian

Let $b_{m,n}(s)$ be a basis spline function of degree m defined on a reference meridian with a knot sequence $\{s_n\}$. It can be proved that the basis spline function is unique and can be expressed as a linear combination of the so-called truncated power functions (see e.g. Schempp (1982)), i.e.

$$b_{m,n}(s) = \sum_{0 \leqslant k \leqslant m+1} a_{k,n}(s - s_{n+k})_+^m, \tag{7}$$

where $(s - s_{n+k})_+ = \sup(s - s_{n+k}, 0)$. To satisfy the continuity, finite support and normal conditions of a basis spline function, the real coefficients $a_{k,n}$ $(k = 0, 1, 2, \ldots, m+1)$ are determined by the following equations:

$$\sum_{0 \leqslant k \leqslant m+1} a_{k,n}(s_l - s_{n+k})^m = 0 \quad (l = n+1, \ldots, n+m+1), \tag{8}$$

$$\sum_{0 \leqslant k \leqslant m+1} a_{k,n}(s_{n+m+1} - s_{n+k})^{m+1} = m+1. \tag{9}$$

Let $f(s,t)$ be a continuous displacement function, for example it may be $u(s,t)$, $v(s,t)$ or $w(s,t)$. When t is constrained on the ith reference meridian, i.e. $t = t_i(s)$, $f(s, t_i(s))$ becomes a continuous function on it. So, $f(s, t_i(s))$ can be approximated by the spline interpolation as follows:

$$f(s, t_i(s)) = \sum_{n=1}^{N_s} \alpha_n b_{m,n}(s), \tag{10}$$

where α_n $(n = 1, 2, \ldots, N_s)$ are interpolation coefficients which should be determined by the specified conditions of $f(s, t_i(s))$ on the reference meridian, and N_s is the total number of basis splines used for the meridian. The specified conditions of $f(s, t_i(s))$ are chosen to be

$$\begin{aligned}\mathbf{f}_i = [&f(s_1, t_i(s_1)), f^{(1)}(s_1, t_i(s_1)), \ldots, f^{(m_l)}(s_1, t_i(s_1)), f(s_2, t_i(s_2)), f(s_3, t_i(s_3)), \ldots, f(s_{N_s-m}, t_i(s_{N_s-m})),\\ &f^{(1)}(s_{N_s-m}, t_i(s_{N_s-m})), \ldots, f^{(m_r)}(s_{N_s-m}, t_i(s_{N_s-m}))]^{\mathrm{T}},\end{aligned} \tag{11}$$

where $m_l = m/2 - \mathrm{mod}(m, 2)$, $m_r = m - m_l - 1$, and $f^{(k)}(s_l, t_i(s_l))$ $(k = 0, 1, 2, \ldots, m_l)$ and $f^{(k)}(s_{N_s-m}, t_i(s_{N_s-m}))$ $(k = 0, 1, 2, \ldots, m_r)$ are values of the displacement function and its derivatives at two ends of a shell element where the kinematic boundary conditions may be enforced.

Substituting these specified conditions in Eq. (11), the obtained $\boldsymbol{\alpha} = [\alpha_1, \alpha_2, \ldots, \alpha_n]^{\mathrm{T}}$ are

$$\boldsymbol{\alpha} = \mathbf{R}^{-1}\mathbf{f}_i, \tag{12}$$

where the elements of $\mathbf{R}$ are

$$\mathbf{R}_{l,k} = \begin{cases} b_{m,k}^{(n)}(s_l) & (l = n+1;\ n = 0, 1, \ldots, m_l;\ k = 1, 2, \ldots, N_s),\\ b_{m,k}(s_n) & (l = n + m_l;\ n = 2, 3, \ldots, N_s - m;\ k = 1, 2, \ldots, N_s),\\ b_{m,k}^{(n)}(s_{N_s-m+1}) & (l = n + N_s - m_r;\ n = 0, 1, \ldots, m_r;\ k = 1, 2, \ldots, N_s). \end{cases} \tag{13}$$

Combining Eqs. (10) and (12), the spline interpolation of $f(s, t_i(s))$ with its specified values is

$$f(s, t_i(s)) = \mathbf{B}_m(s)\mathbf{f}_i, \tag{14}$$

where

$$\mathbf{B}_m(s) = [b_{m,1}(s), b_{m,2}(s), \ldots, b_{m,N_s}(s)]R^{-1}. \tag{15}$$

3.3. Displacement representation in the circumferential direction

When s is fixed, $f(s,t)$ becomes a continuous function in the circumferential t-direction whose values are restricted to $f(s,t_i(s))$ on its junctions with the reference meridians. As in classical TST, only C^0-type continuity is required on displacements $u(s,t)$ and $v(s,t)$, the Lagrangian polynomial interpolation could be used in this direction. Therefore, $u(s,t)$ and $v(s,t)$ can be approximated as

$$u(s,t)=\sum_{i=1}^{i_p}P_i(t,s)u(s,t_i(s)), \tag{16}$$

$$v(s,t)=\sum_{i=1}^{i_p}P_i(t,s)v(s,t_i(s)), \tag{17}$$

where $P_i(t,s)$ $(i=1,2,\ldots,i_p)$ are Lagrangian polynomial functions, for instance when $i_p=4$, they are

$$\begin{aligned}
P_1(\eta)&=(-1+\eta+9\eta^2-9\eta^3)/16,\\
P_2(\eta)&=(9-27\eta-9\eta^2+27\eta^3)/16,\\
P_3(\eta)&=(9+27\eta-9\eta^2-27\eta^3)/16,\\
P_4(\eta)&=(-1-\eta+9\eta^2+9\eta^3)/16,
\end{aligned} \tag{18}$$

where $\eta=2t/l_t(s)$, and $l_t(s)$ is the circumferential arc length of the element at the position s on the meridian.

However, as the Kirchhoff normalcy condition invoked in TST, the requirement of the C^1-type continuity of $w(s,t)$ is necessary. That means the first derivatives of $w(s,t)$ in the circumferential direction (i.e. $\partial w(s,t)/\partial t$) should be used as freedoms at the outside meridians of the element. To satisfy this condition, Hermitian functions are used to interpolate $w(s,t)$ in the circumferential direction, i.e.

$$w(s,t)=\sum_{i=1}^{4}P_{iH}(t,s)w(s,t_i(s)), \tag{19}$$

where

$$\begin{aligned}
P_{1H}(\eta)&=(2-3\eta+\eta^3)/4,\\
P_{2H}(\eta)&=b(1-\eta-\eta^2+\eta^3)/8,\\
P_{3H}(\eta)&=b(-1-\eta+\eta^2+\eta^3)/8,\\
P_{4H}(\eta)&=(2+3\eta-\eta^3)/4,
\end{aligned} \tag{20}$$

where $\eta=2t/l_t(s)$. It should be noted that $P_{1H}(\eta)$ and $P_{2H}(\eta)$ are both associated with reference meridian 1 and related to degrees of freedom corresponding to $w(s,t)$ and $\partial w(s,t)/\partial t$, respectively, so do $P_{4H}(\eta)$ and $P_{3H}(\eta)$ with reference meridian 4 (here, reference meridians 1 and 4 are the two outside reference meridians of the shell element). In summary, by substituting Eq. (14) into Eqs. (16), (17) and (19), the displacement field of an element in TST can be constructed as

$$u(s,t)=\sum_{i=1}^{i_p}P_i(t,s)\mathbf{B}_{m_u}(s)\mathbf{u}_i, \tag{21}$$

$$v(s,t) = \sum_{i=1}^{i_p} P_i(t,s)\mathbf{B}_{m_v}(s)\mathbf{v}_i, \tag{22}$$

$$w(s,t) = \sum_{i=1}^{4} P_{iH}(t,s)\mathbf{B}_{m_w}(s)\mathbf{w}_i. \tag{23}$$

As noted before, $\mathbf{w}_2$ and $\mathbf{w}_3$ in the above equation are not the displacements associated with reference meridians 2 and 3. They are actually $\partial\mathbf{w}_1/\partial t$ and $\partial\mathbf{w}_4/\partial t$, respectively.

4. Stiffness matrix of an element

4.1. Constitutive equations

Within the context of TST, the linear constitutive equations for an arbitrary laminate are

$$\mathbf{F} = \mathbf{L}\mathbf{e}, \tag{24}$$

where

$$\mathbf{F} = [N_s, N_t, N_{st}, M_s, M_t, M_{st}]^{\mathrm{T}}, \tag{25}$$

$$\mathbf{L} = \begin{bmatrix} A_{11} & A_{12} & A_{16} & B_{11} & B_{12} & B_{16} \\ & A_{22} & A_{26} & B_{21} & B_{22} & B_{26} \\ & & A_{66} & B_{61} & B_{62} & B_{66} \\ & & & D_{11} & D_{12} & D_{16} \\ & \text{Sym.} & & & D_{22} & D_{16} \\ & & & & & D_{66} \end{bmatrix}, \tag{26}$$

$$\mathbf{e} = \begin{bmatrix} \frac{\partial u}{\partial s} + \frac{w}{R_s} \\ \frac{\partial v}{\partial t} + \frac{w}{R_t} \\ \frac{\partial u}{\partial t} + \frac{\partial v}{\partial s} \\ -\frac{\partial^2 w}{\partial s^2} + \frac{1}{R_s}\frac{\partial u}{\partial s} \\ -\frac{\partial^2 w}{\partial t^2} + \frac{1}{R_t}\frac{\partial v}{\partial t} \\ -2\frac{\partial^2 w}{\partial s\,\partial t} + \frac{1}{2}\left(\frac{3}{R_t} - \frac{1}{R_s}\right)\frac{\partial v}{\partial s} + \frac{1}{2}\left(\frac{3}{R_s} - \frac{1}{R_t}\right)\frac{\partial u}{\partial t} \end{bmatrix}. \tag{27}$$

The laminate stiffness coefficients in Eq. (26) are defined in the standard way (see e.g. Reddy (1984) and Leissa and Chang (1996)) as

$$(A_{ij}, B_{ij}, D_{ij}) = \int_{-h/2}^{h/2} Q_{ij}(1, z, z^2)\,\mathrm{d}z \quad (i,j = 1,2,6). \tag{28}$$

Q_{ij} $(i,j = 1,2,6)$ are plane-stress reduced stiffness of the fibre-reinforced composite materials or the smart materials in the lay-up (Fig. 1). Obviously, these coefficients are different in different lamination regions $\Omega_{\mathrm{L},l}$ $(l = 1,2,\ldots,n_{\mathrm{L}})$. The explicit expression of the strain vector $\mathbf{e}$ in the specified values of the displacement field can be obtained as follows using Eqs. (21)–(23),

$$\mathbf{e} = \sum_{i=1}^{4} \mathbf{\Phi}_i \mathbf{d}_i, \tag{29}$$

where $\mathbf{d}_i = [\mathbf{u}_i^{\mathrm{T}}, \mathbf{v}_i^{\mathrm{T}}, \mathbf{w}_i^{\mathrm{T}}]^{\mathrm{T}}$ (as noted before, $\mathbf{w}_2$ and $\mathbf{w}_3$ are $\partial\mathbf{w}_1/\partial t$ and $\partial\mathbf{w}_4/\partial t$, respectively, in a TST element) and,

$$\mathbf{\Phi}_i = \begin{bmatrix} P_i\mathbf{B}'_{m_u} & 0 & \frac{1}{R_s}P_{iH}\mathbf{B}_{m_w} \\ 0 & P'_i\mathbf{B}_{m_v} & \frac{1}{R_s}P_{iH}\mathbf{B}_{m_w} \\ P'_i\mathbf{B}_{m_u} & P_i\mathbf{B}'_{m_v} & 0 \\ \frac{1}{R_s}P_i\mathbf{B}'_{m_u} & 0 & -P_{iH}\mathbf{B}''_{m_w} \\ 0 & \frac{1}{R_t}P'_i\mathbf{B}_{m_v} & -P''_{iH}\mathbf{B}_{m_w} \\ \frac{1}{2}(\frac{3}{R_s}-\frac{1}{R_t})P'_i\mathbf{B}_{m_u} & \frac{1}{2}(\frac{3}{R_t}-\frac{1}{R_s})P_i\mathbf{B}'_{m_v} & -2P'_{iH}\mathbf{B}'_{m_w} \end{bmatrix} \tag{30}$$

in which "′" represents the derivative of a function or function vector with respect to its variable.

4.2. Stiffness matrix

The strain energy of an element is

$$U = \frac{1}{2}\sum_{i=1}^{n_{\mathrm{L}}}\int_{\Omega_{\mathrm{L},l}} \mathbf{e}^{\mathrm{T}}\mathbf{L}\mathbf{e}\,\mathrm{d}t\,\mathrm{d}s. \tag{31}$$

Its quadratic form in the specified values of the displacement field is what follows after substituting Eq. (29) into Eq. (31),

$$U = \frac{1}{2}\sum_{i=1}^{n_{\mathrm{L}}}\int_{\Omega_{\mathrm{L},l}}\sum_{i=1}^{4}\sum_{j=1}^{4}\mathbf{d}^{\mathrm{T}}\mathbf{\Phi}_i^{\mathrm{T}}\mathbf{L}_l\mathbf{\Phi}_j\mathbf{d}_j\,\mathrm{d}t\,\mathrm{d}s = \frac{1}{2}\mathbf{d}^{\mathrm{T}}\mathbf{k}\mathbf{d}, \tag{32}$$

where $\mathbf{d} = [\mathbf{d}_1^{\mathrm{T}}, \mathbf{d}_2^{\mathrm{T}}, \mathbf{d}_3^{\mathrm{T}}, \mathbf{d}_4^{\mathrm{T}}]^{\mathrm{T}}$ and,

$$\mathbf{k} = \left[\sum_{i=1}^{n_{\mathrm{L}}}\int_{\Omega_{\mathrm{L},l}}\mathbf{\Phi}_i^{\mathrm{T}}\mathbf{L}_l\mathbf{\Phi}_j\,\mathrm{d}t\,\mathrm{d}s\right]. \tag{33}$$

Matrix $\mathbf{k}$ is the stiffness matrix of an element.

5. Equivalent element nodal forces of thermal load and smart material actuation

For a thin laminated shell element, it is assumed that each one of its layers is in plane-stress state so that the thermal expansion in through-thickness direction is neglected. In the local co-ordinates of each layer of unidirectional composite material, in-plane thermal strains have the following concise expressions:

$$\begin{bmatrix} \varepsilon_{\mathrm{L}}^{(\mathrm{T})} \\ \varepsilon_{\mathrm{T}}^{(\mathrm{T})} \\ \gamma_{\mathrm{LT}}^{(\mathrm{T})} \end{bmatrix} = \begin{bmatrix} \alpha_{\mathrm{L}} \\ \alpha_{\mathrm{T}} \\ 0 \end{bmatrix} T, \tag{34}$$

where α_{L} and α_{T} are thermal expansion coefficients in longitudinal and transverse directions of unidirectional composite layer, respectively, and T is the temperature which may vary with the positions of layers.

Similar to obtaining the stress and moment resultants of elastic strains, the stress and moment resultants of the in-plane thermal strains can be derived as

$$\begin{bmatrix} N_s^{(T)} \\ N_t^{(T)} \\ N_{st}^{(T)} \end{bmatrix} = \sum_{n=1}^{n_l} \mathbf{T}_s(\theta_n) \begin{bmatrix} Q_{11} & Q_{12} & Q_{16} \\ Q_{21} & Q_{22} & Q_{26} \\ Q_{61} & Q_{62} & Q_{66} \end{bmatrix}_n \begin{bmatrix} \varepsilon_L^{(T)} \\ \varepsilon_T^{(T)} \\ \gamma_{LT}^{(T)} \end{bmatrix}_n (h_n - h_{n-1}), \tag{35}$$

$$\begin{bmatrix} M_s^{(T)} \\ M_t^{(T)} \\ M_{st}^{(T)} \end{bmatrix} = \frac{1}{2} \sum_{n=1}^{n_l} \mathbf{T}_s(\theta_n) \begin{bmatrix} Q_{11} & Q_{12} & Q_{16} \\ Q_{21} & Q_{22} & Q_{26} \\ Q_{61} & Q_{62} & Q_{66} \end{bmatrix}_n \begin{bmatrix} \varepsilon_L^{(T)} \\ \varepsilon_T^{(T)} \\ \gamma_{LT}^{(T)} \end{bmatrix}_n (h_n^2 - h_{n-1}^2), \tag{36}$$

where n_l is the number of layers in a thermal region $\Omega_{T,l}$ bordered by two meridians and two circumferential arcs, of which the temperatures of its four corners at top and bottom surfaces are characterized by T_i^U, T_i^D $(i = 1–4)$ (Fig. 3), $\mathbf{T}_s(\theta_n)$ is a stress transformation matrix from the local co-ordinates of the nth layer to the natural co-ordinates of the element, Q_{ij} $(i, j = 1, 2, 6)$ are plane-stress reduced stiffness coefficients as used before, h_n is the distance from the middle surface to the lower surface of the nth layer.

The interpolation of temperature field for a thermal region $\Omega_{T,l}$ is given by

$$T(s,t,z) = \begin{cases} T^D(s,t) + (T^U(s,t) - T^D(s,t))(z/h + 0.5)^\beta, & T^U(s,t) \geqslant T^D(s,t), \\ T^U(s,t) + (T^D(s,t) - T^U(s,t))(0.5 - z/h)^\beta, & T^D(s,t) \geqslant T^U(s,t), \end{cases} \tag{37}$$

where β is a parameter characterizing the temperature distribution through shell thickness, h, and linear interpolations are used for calculating $T^U(s,t)$ and $T^D(s,t)$, i.e.

$$T^U(s,t) = T_1^U + (T_2^U - T_1^U)\frac{s - s_1}{s_2 - s_1} + \frac{t - t_1}{t_2 - t_1}\left[(T_3^U - T_1^U) + (T_4^U - T_3^U - T_2^U + T_1^U)\frac{s - s_1}{s_2 - s_1}\right], \tag{38}$$

$$T^D(s,t) = T_1^D + (T_2^D - T_1^D)\frac{s - s_1}{s_2 - s_1} + \frac{t - t_1}{t_2 - t_1}\left[(T_3^D - T_1^D) + (T_4^D - T_3^D - T_2^D + T_1^D)\frac{s - s_1}{s_2 - s_1}\right]. \tag{39}$$

Finally, the potential energy of the thermal strains can be derived as

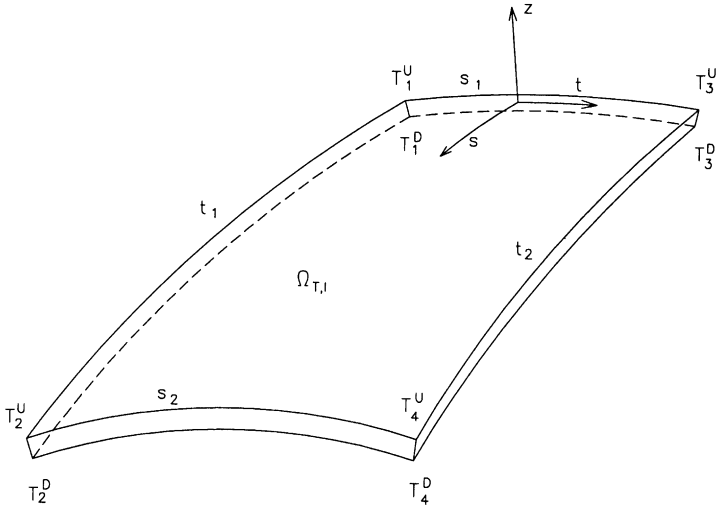

Fig. 3. Characteristics of a thermal region.

$$U_{\mathrm{T}} = -\sum_{l=1}^{n_{\mathrm{T}}} \int_{\Omega_{\mathrm{T},l}} \sum_{i=1}^{4} \mathbf{d}_i^{\mathrm{T}} \boldsymbol{\Phi}_i^{\mathrm{T}} \mathbf{F}^{(\mathrm{T})} \,\mathrm{d}t\,\mathrm{d}s = -\mathbf{d}^{\mathrm{T}} \mathbf{f}_e^{(\mathrm{T})}, \tag{40}$$

where $\mathbf{F}^{(\mathrm{T})}$ is the stress and moment resultants from the thermal strains, i.e.

$$\mathbf{F}^{(\mathrm{T})} = [N_s^{(\mathrm{T})}, N_t^{(\mathrm{T})}, N_{st}^{(\mathrm{T})}, M_s^{(\mathrm{T})}, M_t^{(\mathrm{T})}, M_{st}^{(\mathrm{T})}]^{\mathrm{T}}. \tag{41}$$

n_{T} is the total number of thermal regions and $\mathbf{f}_e^{(\mathrm{T})}$ is the equivalent element nodal forces resulted from thermal loads, whose explicit expression is

$$\mathbf{f}_e^{(\mathrm{T})} = \left[\sum_{l=1}^{n_{\mathrm{T}}} \int_{\Omega_{\mathrm{T},l}} \boldsymbol{\Phi}_i^{\mathrm{T}} \mathbf{F}^{(\mathrm{T})} \,\mathrm{d}t\,\mathrm{d}s \right]. \tag{42}$$

The exact procedure as illustrated above can also be applied to derive the equivalent element nodal forces $\mathbf{f}_e^{(\mathrm{A})}$ resulted from the induced actuation strains. For layered type of smart materials, only the in-plane induced actuation strains are considered. They have a succinct relationship with the external electric field E_3 as follows:

$$\begin{bmatrix} \varepsilon_1^{(\mathrm{A})} \\ \varepsilon_2^{(\mathrm{A})} \\ \gamma_{12}^{(\mathrm{A})} \end{bmatrix} = \begin{bmatrix} d_{31} \\ d_{32} \\ 0 \end{bmatrix} E_3, \tag{43}$$

where d_{31} and d_{32} are mechanical/electrical coupling coefficients.

The stress and moment resultants, $\mathbf{F}^{(\mathrm{A})}$, of the induced actuation strains have the similar expressions as Eqs. (35), (36) and (41), in which the thermal strains are replaced by the induced actuation strains and the summations there are now over the smart material layers in the actuation regions $\Omega_{\mathrm{A},l} (l = 1, 2, \ldots, n_{\mathrm{A}})$. Then, referring to Eq. (42), the explicit expression of $\mathbf{f}_e^{(\mathrm{A})}$ is

$$\mathbf{f}_e^{(\mathrm{A})} = \left[\sum_{l=1}^{n_{\mathrm{A}}} \int_{\Omega_{\mathrm{A},l}} \boldsymbol{\Phi}_i^{\mathrm{T}} \mathbf{F}^{(\mathrm{A})} \,\mathrm{d}t\,\mathrm{d}s \right]. \tag{44}$$

6. Control schemes

The structural stiffness matrix and nodal force vector can be assembled by those of its elements in the standard way using direct stiffness method. The final equilibrium equation of structures under thermal loads and active control forces can be expressed as

$$\mathbf{KD} = \mathbf{f}^{(\mathrm{T})} + \mathbf{f}^{(\mathrm{A})}(\mathbf{E}), \tag{45}$$

where $\mathbf{K}$ and $\mathbf{D}$ are structural stiffness matrix and displacement vector, respectively; $\mathbf{f}^{(\mathrm{T})}$ and $\mathbf{f}^{(\mathrm{A})}(\mathbf{E})$ are structural nodal force vectors corresponding to thermal loads and induced strain actuation, of which the latter has been expressed explicitly as a function of active control input vector $\mathbf{E}$ that consists of the voltage of electric field for each of the actuators.

The deformation control discussed here aims at making the overall structural displacement $\mathbf{D}$ be as small as possible with the use of control actuators by choosing proper control input vector $\mathbf{E}$ for them. From Eq. (45), it is obvious that structural displacements would be zero if the above two types of structural nodal forces could exactly balance with each other. Unfortunately, this only happens when there are infinite sensors and actuators located at all points of a structure, which could not be realized in real practice. When there are only finite sensors and actuators, the induced strain actuation cannot completely balance the

thermal load. Therefore, non-zero overall structural displacements are inevitable. Finding a way to minimize these displacements is the task of designing the control schemes. The following will introduce a control scheme based on strain measurements. A strain sensor (in numerical simulations is a position where a strain component is calculated) is placed at the centre of a co-located actuator which is bonded on or embedded in a shell structure. In the kth control step for which control input of electric fields $\mathbf{E}^{(k)}$ has already taken place, the measured/calculated structural strains under thermal loads and current control actuation are $\Xi^{(k)}$. To reduce these strains, additional induced actuation strains need to be produced by supplying additional electric fields $\Delta\mathbf{E}^{(k)} = \Xi^{(k)}/d_{31}$ (or $\Xi^{(k)}/d_{32}$) to the actuators. Thus, the ideal total control needed in this step is $\mathbf{E}^{(k)} + \Delta E^{(k)}$. To consider the effect of finite number of sensors and actuators, a gain parameter needs to be included in the control algorithm. Therefore, the following control schemes with respect to different uses of the gain parameter are suggested:

1. Algorithm based on ideal total input:

Meridional control $\mathbf{E}^{(k+1)} = c_s(\mathbf{E}^{(k)} + \Delta\mathbf{E}^{(k)}) = c_s(\mathbf{E}^{(k)} + \Xi_s^{(k)}/d_{31})$,

Circumferential control $\mathbf{E}^{(k+1)} = c_t(\mathbf{E}^{(k)} + \Delta\mathbf{E}^{(k)}) = c_t(\mathbf{E}^{(k)} + \Xi_t^{(k)}/d_{32})$.

2. Algorithm based on ideal additional input:

Meridional control $\mathbf{E}^{(k+1)} = \mathbf{E}^{(k)} + c_s\Delta\mathbf{E}^{(k)} = \mathbf{E}^{(k)} + c_s\Xi_s^{(k)}/d_{31}$,

Circumferential control $\mathbf{E}^{(k+1)} = \mathbf{E}^{(k)} + c_t\Delta\mathbf{E}^{(k)} = \mathbf{E}^{(k)} + c_t\Xi_t^{(k)}/d_{32}$,

where c_s and c_t are control gain parameters, $\Xi_s^{(k)}$ and $\Xi_t^{(k)}$ are structural strain responses whose components can be calculated from structural displacements by the following equations:

$$\varepsilon_s = \left(1 + \frac{z}{R_s}\right)\frac{\partial u}{\partial s} - z\frac{\partial^2 w}{\partial s^2} + \frac{w}{R_s}, \tag{46}$$

$$\varepsilon_t = \left(1 + \frac{z}{R_t}\right)\frac{\partial v}{\partial t} - z\frac{\partial^2 w}{\partial t^2} + \frac{w}{R_t}. \tag{47}$$

Their explicit expressions in terms of the specified values of the displacement field can be derived as follows by substituting Eqs. (21)–(23) into Eqs. (46) and (47):

$$\begin{bmatrix} \varepsilon_s \\ \varepsilon_t \end{bmatrix} = \sum_{i=1}^{4} \mathbf{\Phi}_i^{(S)}\mathbf{d}_i, \tag{48}$$

where

$$\mathbf{\Phi}_i^{(S)} = \begin{bmatrix} \left(1 + \frac{1}{R_s}\right)P_i\mathbf{B}'_{m_u} & 0 & \frac{1}{R_s}P_{iH}\mathbf{B}_{m_w} - zP_{iH}\mathbf{B}''_{m_w} \\ 0 & \left(1 + \frac{1}{R_t}\right)P_i\mathbf{B}'_{m_v} & \frac{1}{R_s}P_{iH}\mathbf{B}_{m_w} - zP''_{iH}\mathbf{B}_{m_w} \end{bmatrix}. \tag{49}$$

For simplicity in deriving the control schemes as illustrated above, the assumption is made that the co-ordinates of actuator material coincide with the natural co-ordinates of shell of revolution, otherwise a strain transformation matrix will be involved.

It is expected that the algorithm based on ideal total input be used in a situation in which a significant portion of structural surface is left uncontrolled and the algorithm based on ideal additional input be used when most of structural surface is under control.

7. Numerical simulations

To test the numerical procedure developed in this paper, a wide range of applications are discussed below, which include the controlled deformation of a composite beam and plate, thermal deformation and its control of a composite plate and a paraboloid shell.

7.1. Controlled deformation of a cantilever beam-plate

The beam-plate is made of aluminium with Young's modulus $E_b = 68.94$ GPa. Its dimensions are length $L = 450$ mm, width $d = 100$ mm and thickness $h_b = 3.173$ mm. On its upper and lower surfaces, two layers of thickness $h_a = 0.25$ mm of piezoelectric materials with properties, Young's modulus $E_a = 63$ GPa and electrical/mechanical coupling coefficient $d_{31} = 2.54 \times 10^{-7}$ mmV^{-1} are bonded by two thin adhesive layers with Young's modulus $E_h = 3.068$ GPa and thickness $h_h = 0.1016$ mm. The beam deforms under the actuation of the piezoelectrics when external electric fields are supplied to them. The exact solution of the tip deflection of this beam exists when pure bending actuation is in force, which has the following expression:

$$w(L) = \frac{1}{2} L^2 \frac{M}{D}, \tag{50}$$

where D is the bending stiffness as defined in Eq. (26) and M is the moment resultant of the induced actuation strain which can be calculated using an equation similar to Eq. (36). This beam-plate is analyzed with the proposed procedure in which only one element with seven evenly spaced knots is involved. The numerical result for the tip deflection is 2.05 mm, which is quite close to the analytical result 2.03 mm obtained with Eq. (50).

7.2. Controlled deformation of a cantilevered laminated composite plate

The unidirectional composite material in this $[0°/\pm 45°]_s$ laminated plate has the properties as Young's moduli $E_L = 150$ GPa, $E_T = 9$ GPa and Poisson ratio $v_{LT} = 0.3$. The geometric definitions of this plate are shown in Fig. 4. The material properties of the actuating layers are the same as that given in the first example. A constant voltage (394 V/mm) with an opposite sign was applied to the piezoelectrics on each side of the plate. This plate was first investigated by Crawly and de Luis (1987) experimentally. Later,

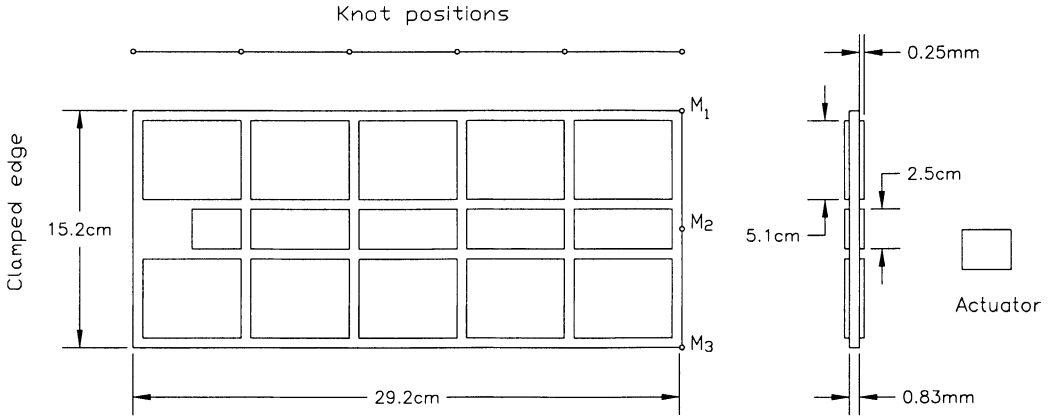

Fig. 4. A cantilevered composite plate containing surface-bonded distributed piezoelectric actuators (description of the experimental set-up by Crawly).

Ha et al. (1992) generated a numerical simulation for it using an eight-node 32 degrees-of-freedom brick element including incompatible modes. In their studies, the following three nondimensional deflections are calculated using either test results or finite element predictions:

(a) longitudinal bending: $W_L = M_2/C$,
(b) transverse bending: $W_T = (M_2 - (M_1 + M_3)/2)/C$,
(c) lateral twisting deformation: $W_R = (M_1 - M_3)/C$,

where C is the width of the plate, and M_1, M_3 and M_2 are the lateral deflections measured along the two edges and the centreline, respectively, as shown in Fig. 4.

In the analysis using the proposed procedure, 24 elements are used. Each of them runs the full length of the plate. The middle plate-strip with narrower actuators on its top and bottom surfaces uses four equal-width elements, each of the two side plate-strips with wider actuators uses eight equal-width elements, and each of the four plate strips without actuators on them uses one element. The knot positions in all elements are shown in Fig. 4. The calculated three deflections defined above are depicted in Fig. 5. They are quite close to what were given by Ha et al. (1992).

7.3. Shape control of a simply supported laminated composite plate

This example was developed by Ha et al. (1992) based on the original set-up of the composite plate used in the experiment of Crawly and de Luis (1987) as illustrated in Fig. 4. The lay-up of the composite plate and the properties of its unidirectional composite material as well as piezoelectrics are the same as those used in the above example. The thermal expansion coefficients are $\alpha_L = 1.1$ μm/m°C, $\alpha_T = 25.2$ μm/m°C for the unidirectional composite material and $\alpha_1 = \alpha_2 = 0.9$ μm/m°C for the piezoelectrics. The geometric definitions of the plate are illustrated in Fig. 6. This plate is simply supported at its two shorter edges whilst its two longer edges are free. The temperatures at the top and bottom surfaces of the plate are 50°F and −50°F, respectively.

In the numerical simulations of Ha et al. (1992), the input to each actuator is applied in the same way as in the above example, i.e. a constant voltage with an opposite sign was applied to the piezoelectrics on each side of the plate. It was found that by supplying 61 V to all of the piezoceramics, the entire deformation shape of the structure was nearly flat. To test the proposed procedure in this case, 19 equal-width elements running the full length of the plate are used, and 13 equal-spaced knots are placed in each element. The calculated centreline deflections of an uncontrolled plate and a controlled plate with actuator voltages of 31 and 61 V, respectively, are depicted in Fig. 7. Indeed, when 61 V was supplied to all piezoceramics, the centreline deflections are very small. To give more information about the controlled deformations of the plate, the free-edge deflections are also calculated and shown in Fig. 7. The exaggerated configurations of this plate in each case are plotted in Fig. 8.

This shape control problem is also investigated using the proposed control schemes based on a control algorithm involving strain measurement. As there is a significant portion of the plate surface that is not controlled and the longitudinal bending is the major deformation, the algorithm based on ideal total input using meridional bending strain calculation is employed. The control gain parameter is chosen to be 1.2. This results in a very good convergent behaviour for the control process, which is shown in Fig. 9. To compare with the above results obtained using the uniform control scheme, the centreline and free-edge deflections are also calculated and they are depicted in Fig. 10. It can be seen from Figs. 7 and 10 that although the maximum centreline deflections under the two control schemes are not very different, the free-edge deflections under the proposed control scheme are much smaller than that under the uniform control scheme. This means the overall controlled deformation shape achieved using the proposed control scheme is flatter than what is shown in Fig. 8(c). The exaggerated configuration of this plate under the proposed control scheme is plotted in Fig. 11.

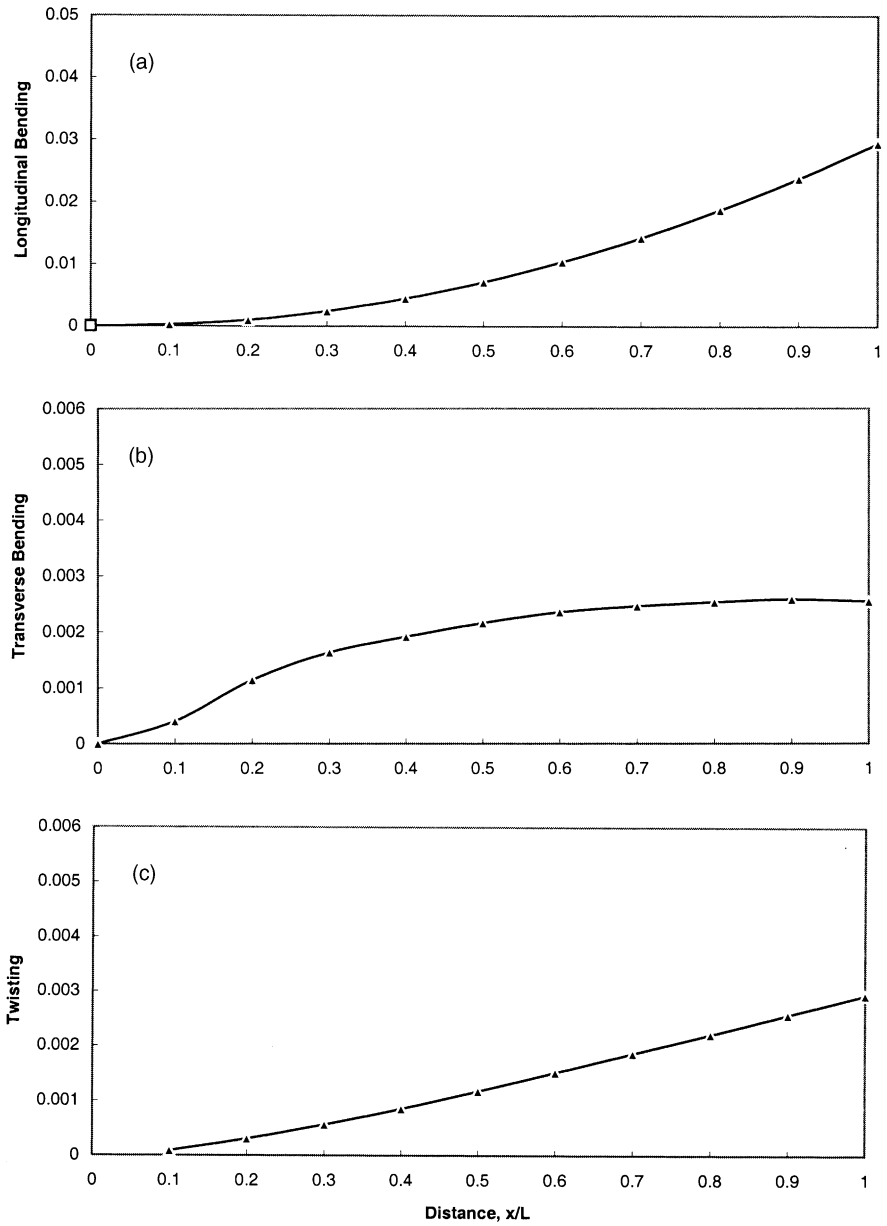

Fig. 5. (a) Longitudinal bending W_L, (b) transverse bending W_T, and (c) lateral twisting W_R of a cantilevered $[0°/\pm 45°]_s$ composite plate.

7.4. Compensation for thermal deformation of a paraboloid composite shell using distributed structural actuation

The geometric definitions of the shell are illustrated in Fig. 12. Its lay-up is $[0°/\pm 45°]_s$. The properties of its unidirectional composite material as well as piezoelectrics and their thicknesses remain the same as that used for the composite plate in Fig. 6. Because of the coupling between membrane extension and bending

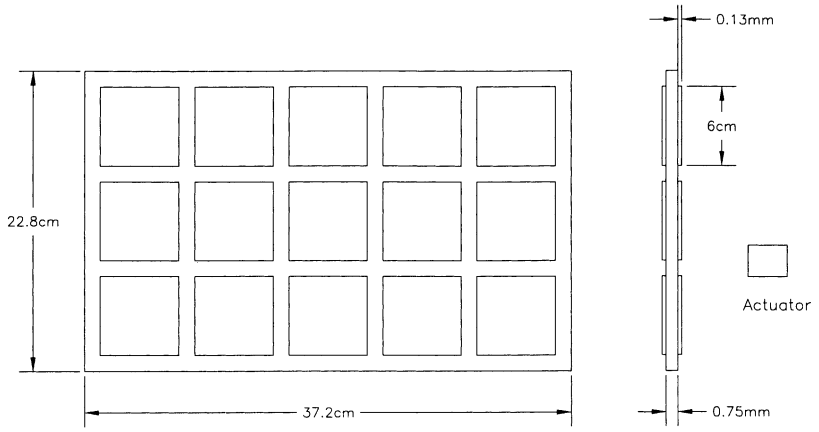

Fig. 6. A controlled actuator composite plate exposed to elevated environment.

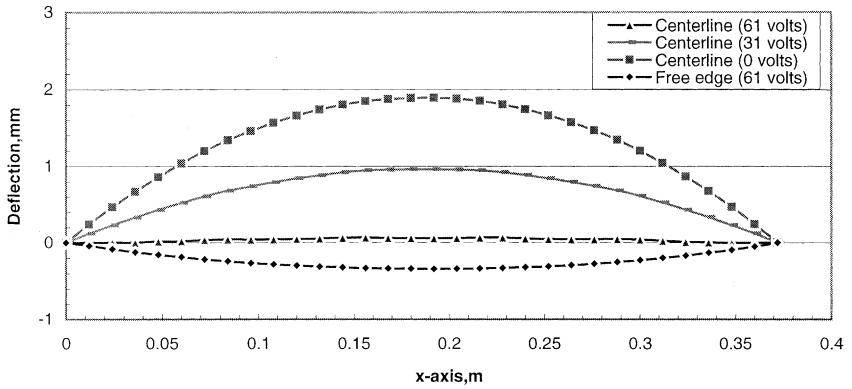

Fig. 7. Calculated deflections of an actuator composite plate exposed to elevated environment.

deflection in the deformation behaviour of a shell, it is expected that its deformations are difficult to be controlled if a significant portion of its surface is left free. Therefore, densely packed distributed structural actuators are used and the gaps between them are neglected. As illustrated in Fig. 12, nine rings of actuators with meridional length 5 cm are used for the paraboloid shell of which only a small core area of its surface is left uncontrolled. Each of the rings has 64 same-sized actuators. This paraboloid shell models an antenna with focus 81.06 cm which is supported by three fixed points, i.e. A, B and C in Fig. 12. Its thermal deformation control in the following three thermal load cases is investigated:

(a) The temperature of the lefthalf outside surface of the antenna is 50°C whilst those of its inside and righthalf outside surfaces are −20°C. This temperature distribution models the antenna facing a thermal source from the left.
(b) The temperatures of the inside and outside surfaces of the antenna are −20°C and 50°C, respectively, which models the antenna facing a thermal source at the back.
(c) The temperatures of the inside and outside surfaces of the antenna are 50°C and −20°C, respectively, which models the antenna facing a thermal source in the front.

In the analysis using the present approach, 64 elements running the full meridional length of the shell are used, and 13 equal-spaced knots are placed in each element. As the actuators are densely packed, the

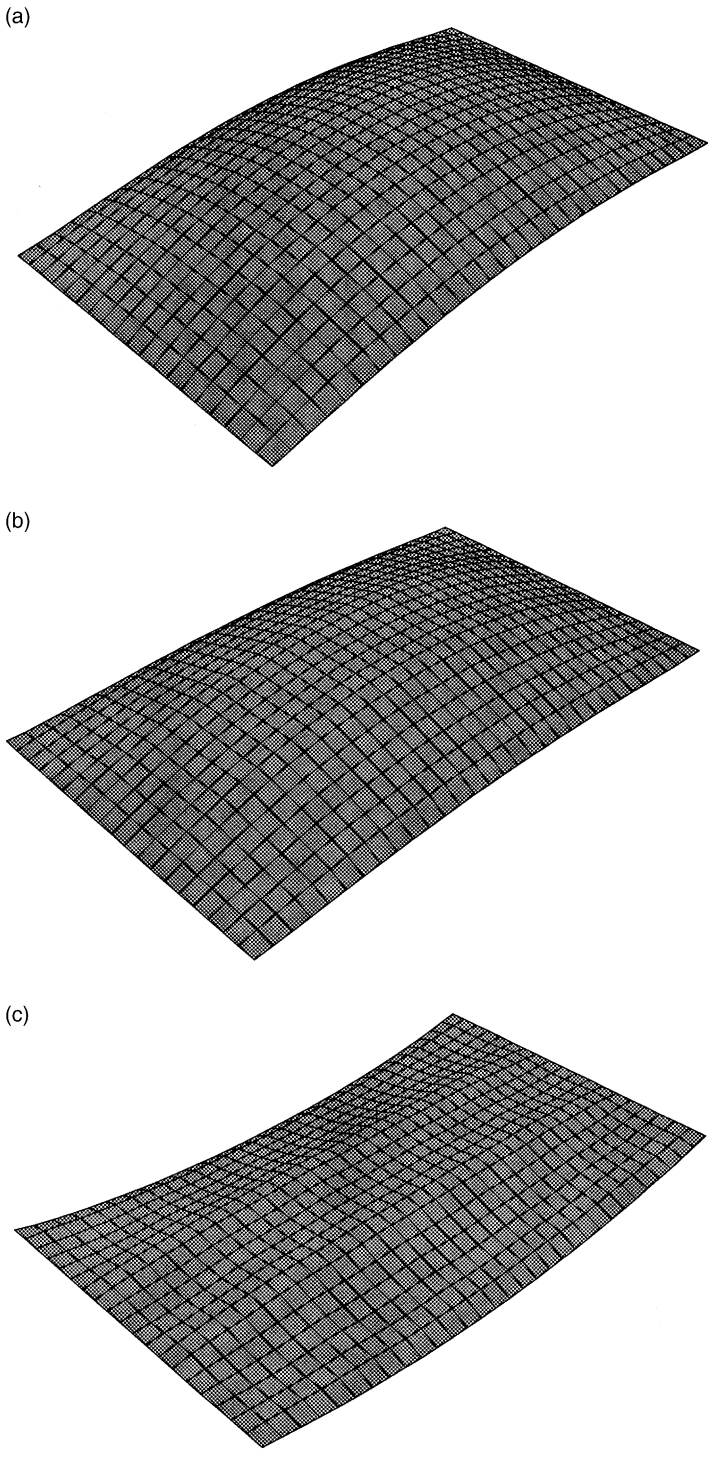

Fig. 8. Exaggerated configurations of an actuator composite plate exposed to elevated environment ((a) uncontrolled, (b) controlled with 31 V and (c) controlled with 61 V).

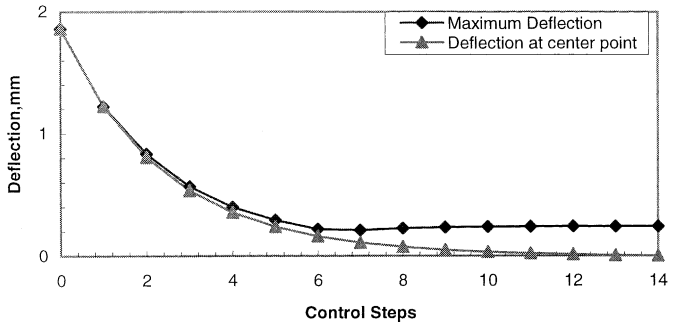

Fig. 9. Convergent deflection processes of an actuator composite plate exposed to elevated environment using meridional control.

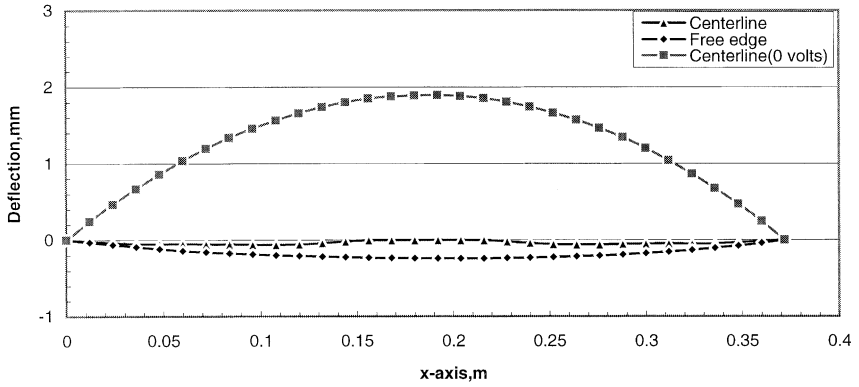

Fig. 10. Calculated deflections of an actuator composite plate exposed to elevated environment using meridional control.

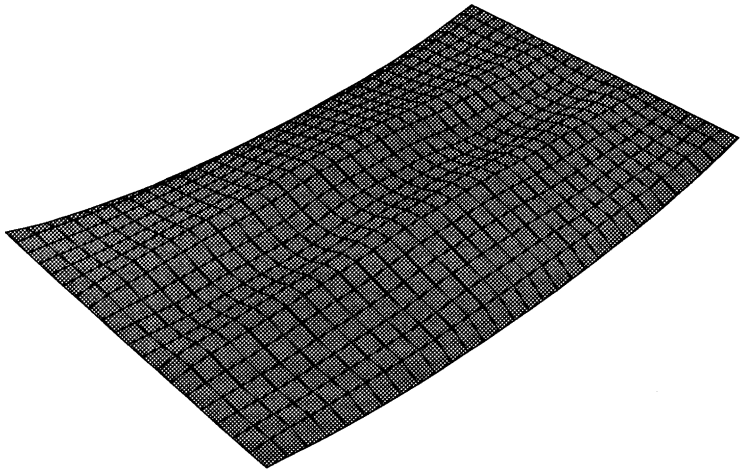

Fig. 11. Exaggerated configurations of an actuator composite plate exposed to elevated environment using meridional control.

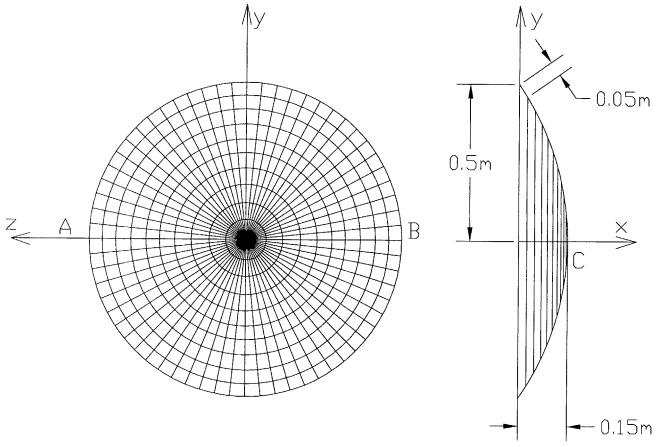

Fig. 12. An actuator composite paraboloid shell.

control scheme is then chosen as the one based on ideal additional input, for which both meridional and circumferential control with control gain parameter 2.0 are employed. Various generated results are shown in the following figures. First, the normal deflections of the outside circumferential edge are depicted in Fig. 13. Because of the large circumferentially distorted deformation (Fig. 19(a)), it was found that meridional control cannot lead to a satisfied controlled deformation for the shell in the first thermal load case. The corresponding results are therefore omitted. However, in this situation, the circumferential control exhibits good control effect which can suppress the thermal deformations considerably. In the second and third thermal load cases, meridional control shows better control effect than the circumferential one. This is mainly because there is only single curvature bending along shell meridians in these two load cases.

Second, the normal deflections along the meridians are plotted in Figs. 14–16. These figures show clearly that the normal deflection at a location where densely packed distributed structural actuation is present (i.e. in the ring-shape area with total meridional length of 0.45 cm) can be effectively controlled although there is influence of the boundary conditions or deformations of the uncontrolled shell surface near the borders of this area. In contrast, the normal deflection of the free shell surface (i.e. the inner core area) can hardly be controlled. They remain almost the same both before and after the control action.

The convergence of the control processes is shown in Fig. 17 in which the decrease of the absolute maximum displacements is drawn against the increase of the control steps. It is noted that the convergent values of the absolute maximum displacements are those happening in the small core area where active control is absent.

The exaggerated final configurations of an uncontrolled and a controlled actuator composite paraboloid shell in different load cases and under different control schemes are depicted in Figs. 18–20. For comparison, the original ideal configuration of this paraboloid shell is also plotted in Fig. 21.

8. Conclusions

A control algorithm based on co-located strain measurement is developed for structural shape control using distributed structural actuation. Its success lies in the fact that an undeformed structure must have a zero strain state and vice versa. Therefore, if the strains at many locations on a structure could be controlled to approach zero, the structural shape would then be quite close to its undeformed one. Obviously, the effectiveness of control increases with the number of sensors and actuators used all over a structure.

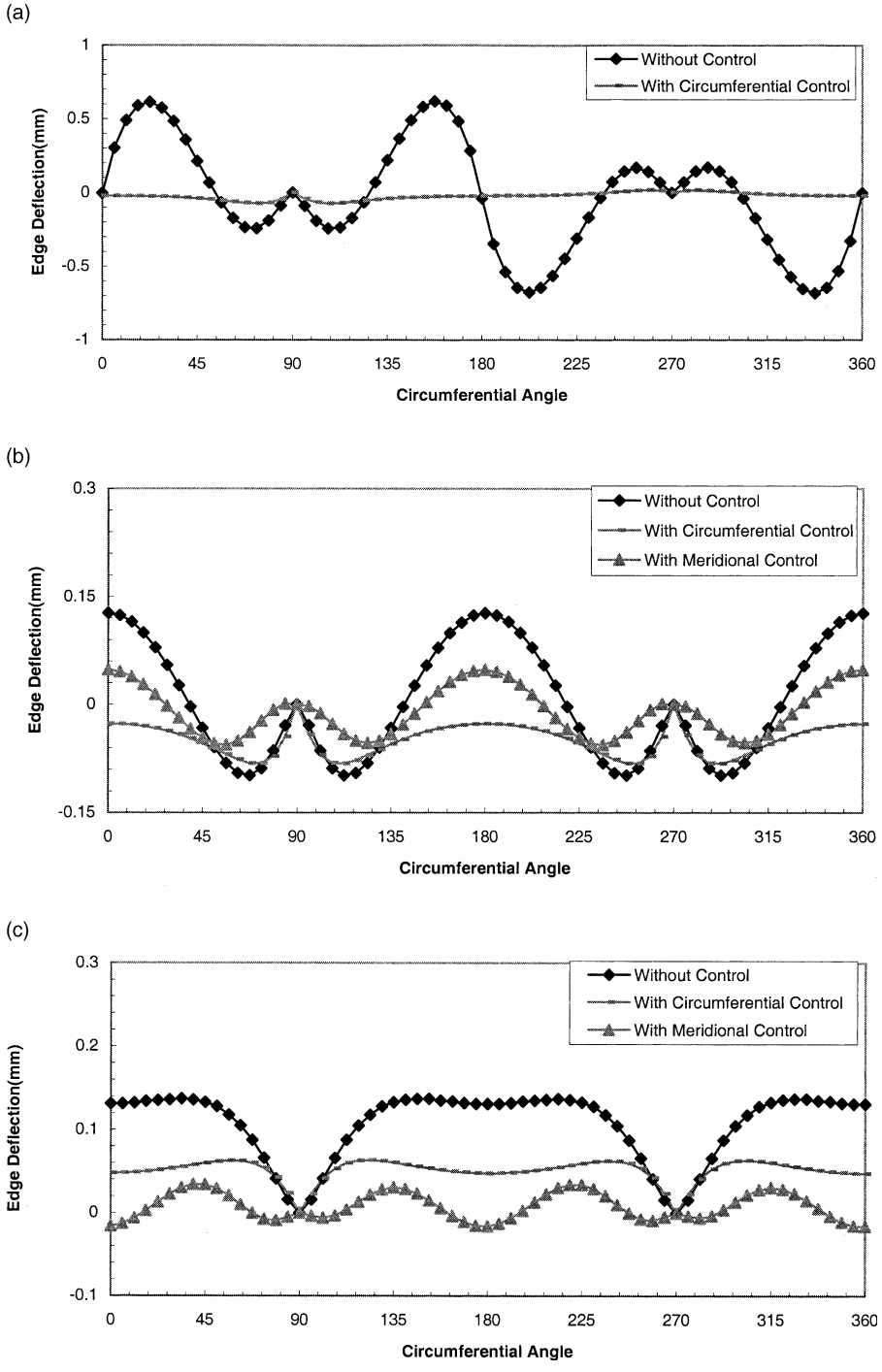

Fig. 13. Normal deflections on the outside circumferential edge ((a) first, (b) second and (c) third thermal load case).

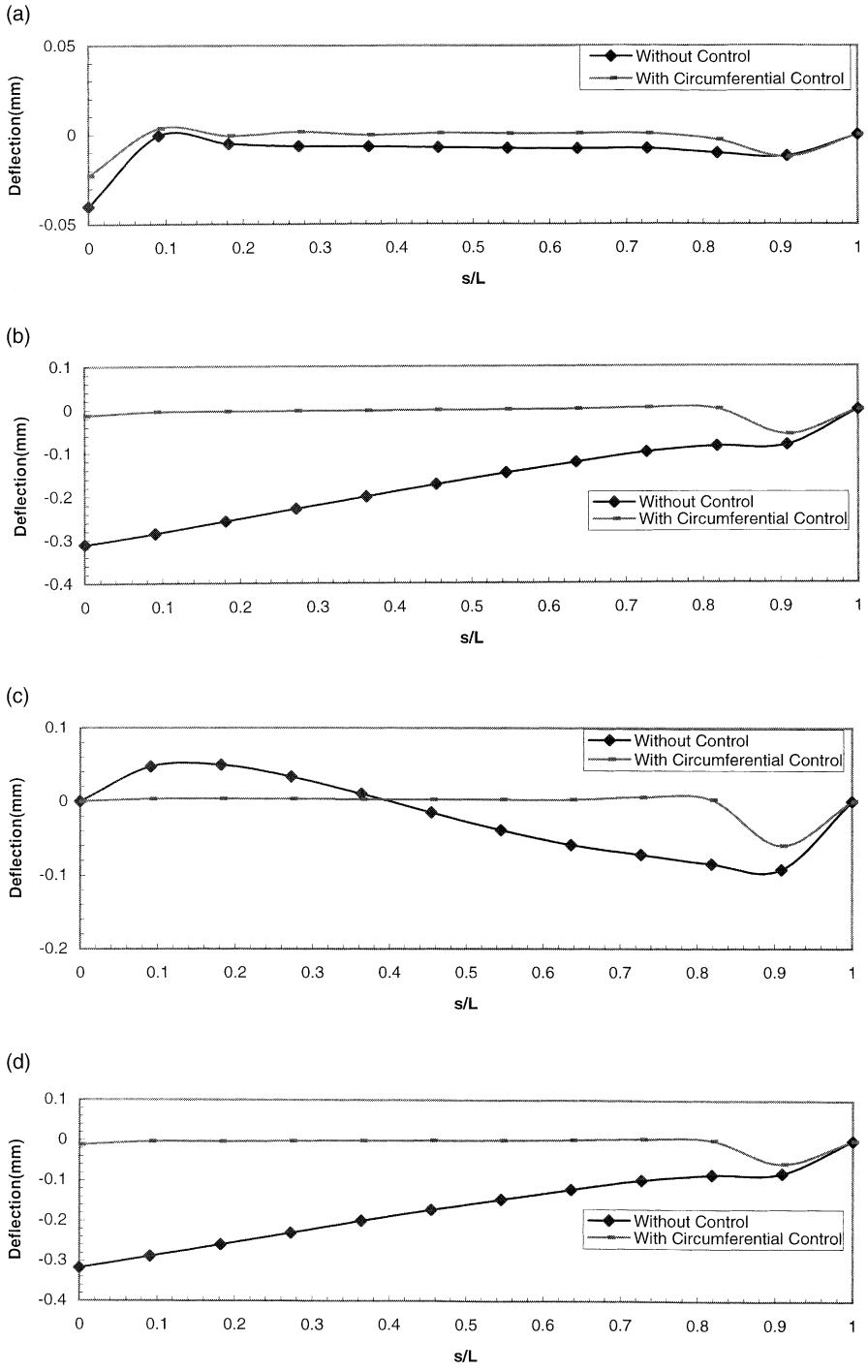

Fig. 14. Normal deflections on the meridians in the first thermal load case (circumferential angle: (a) 0°, (b) 45°, (c) 90°, (d) 135°, (e) 180°, (f) 225°, (g) 270° and (h) 315°).

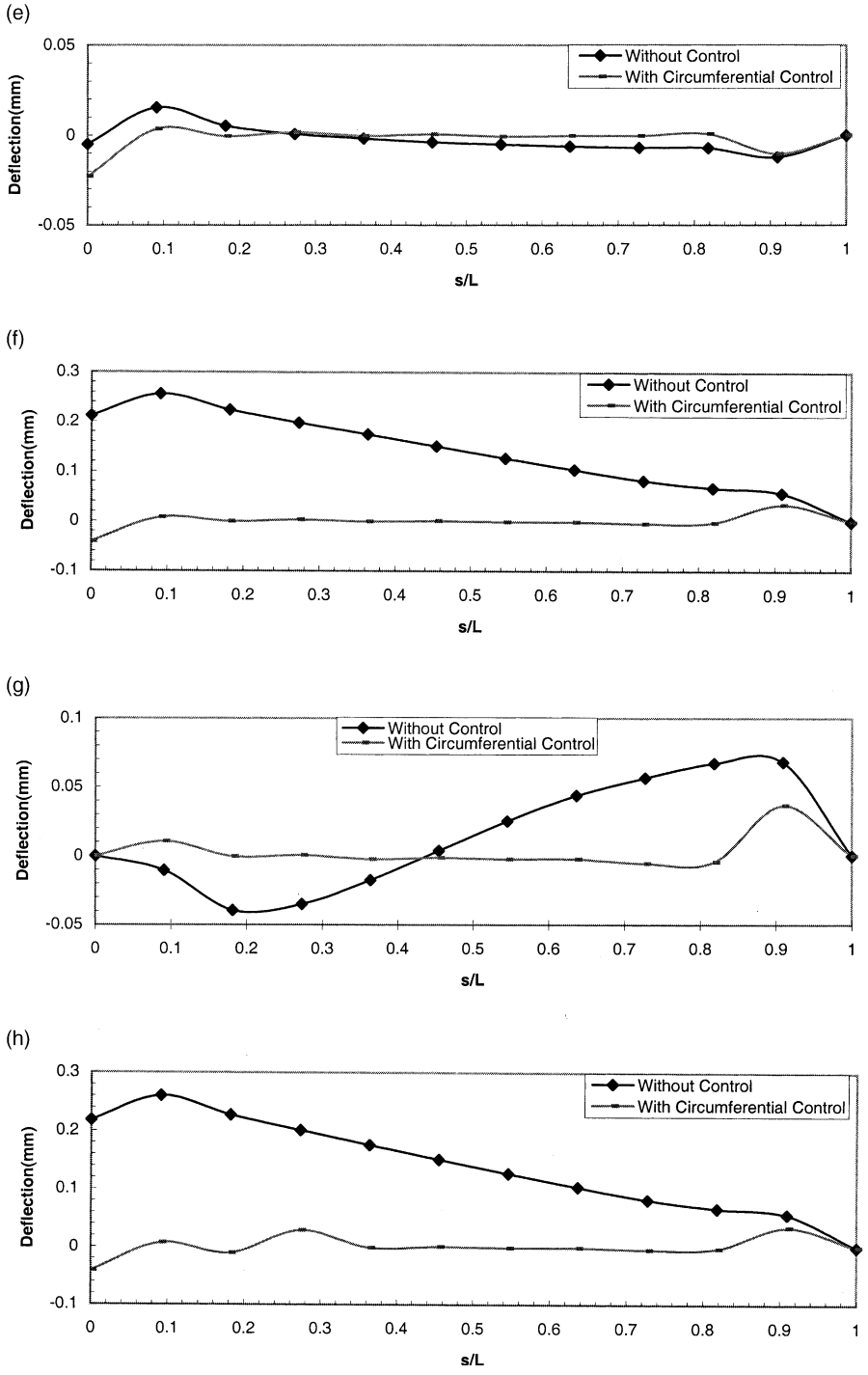

Fig. 14. (*continued*).

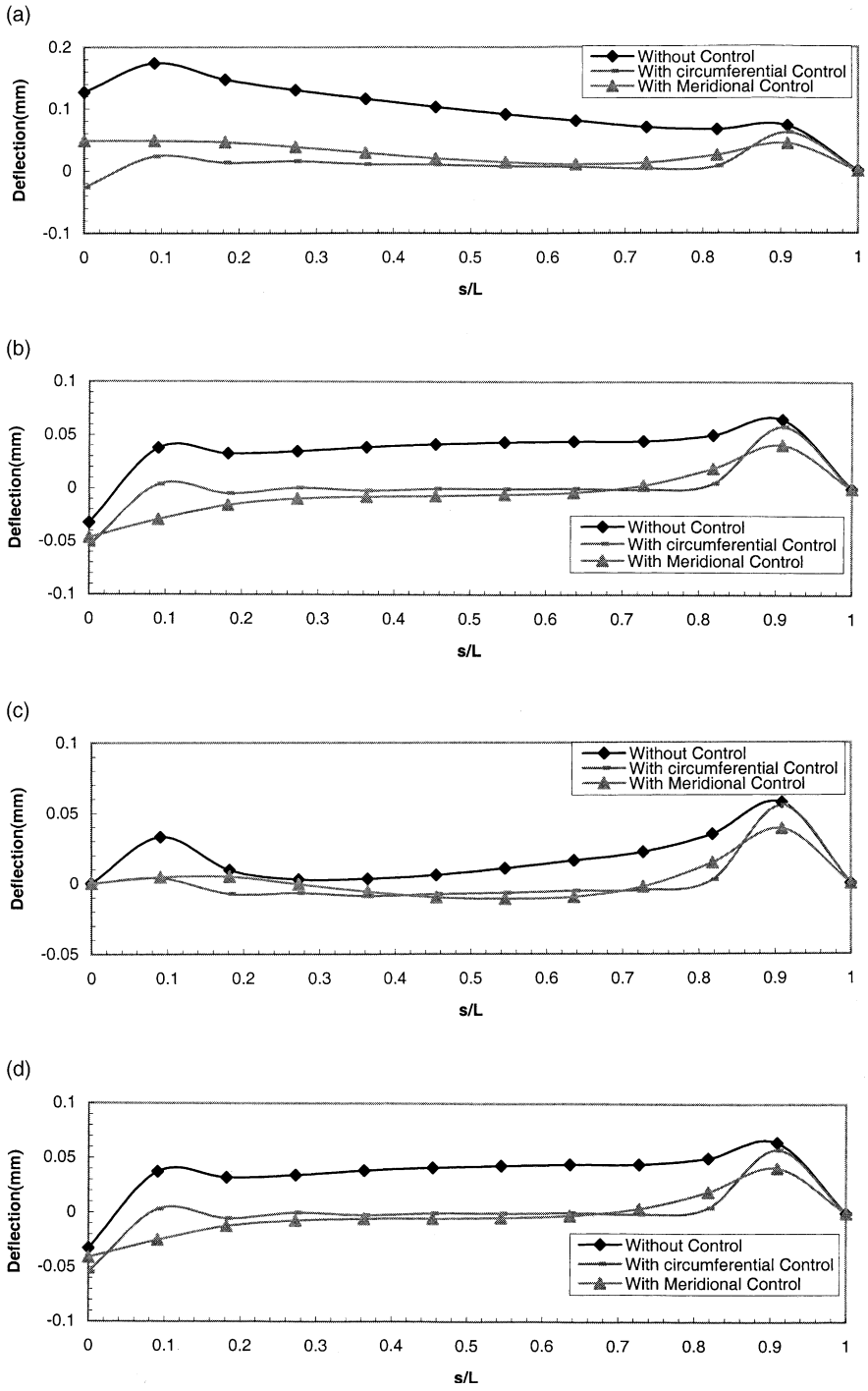

Fig. 15. Normal deflections on the meridians in the second thermal load case (circumferential angle: (a) 0°, (b) 45°, (c) 90° and (d) 135°).

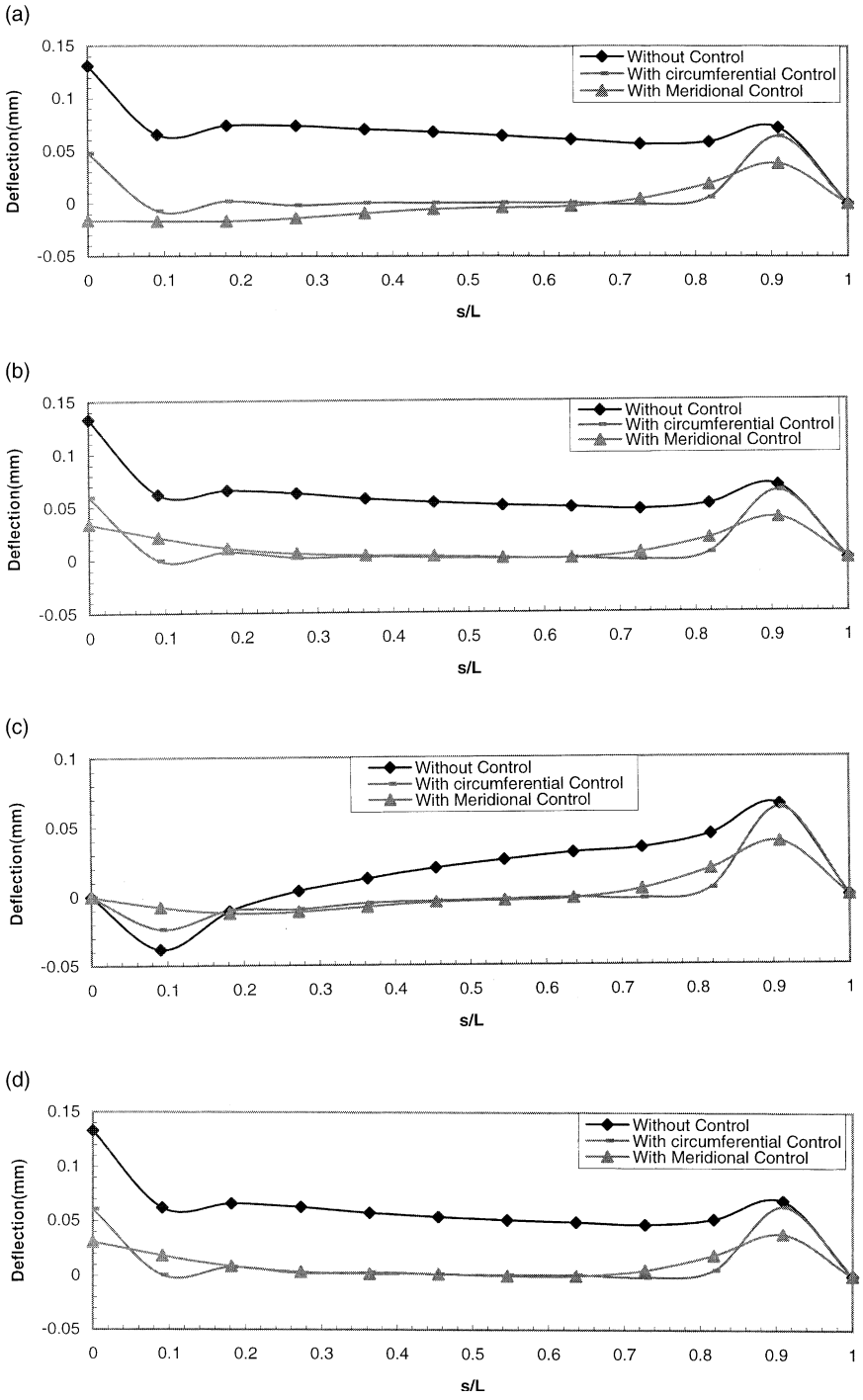

Fig. 16. Normal deflections on the meridians in the third thermal load case (circumferential angle: (a) 0°, (b) 45°, (c) 90° and (d) 135°).

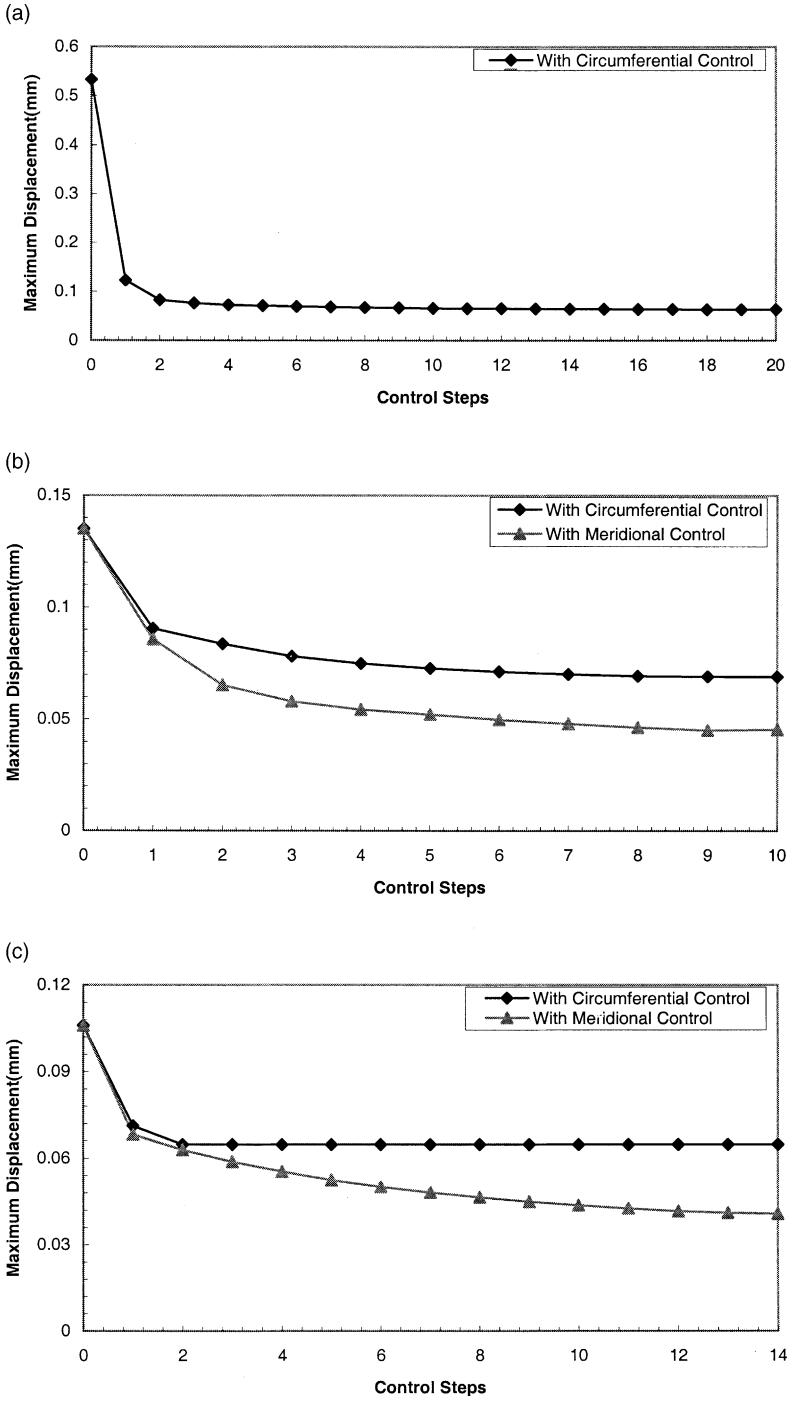

Fig. 17. Convergent deflection processes of an actuator composite paraboloid shell ((a) first, (b) second and (c) third thermal load case).

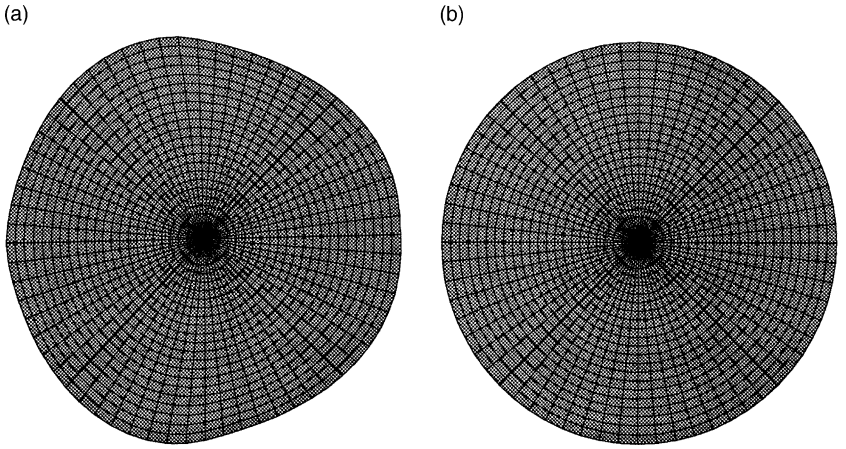

Fig. 18. Exaggerated configurations of an actuator composite paraboloid shell in the first load case ((a) uncontrolled and (b) circumferential control).

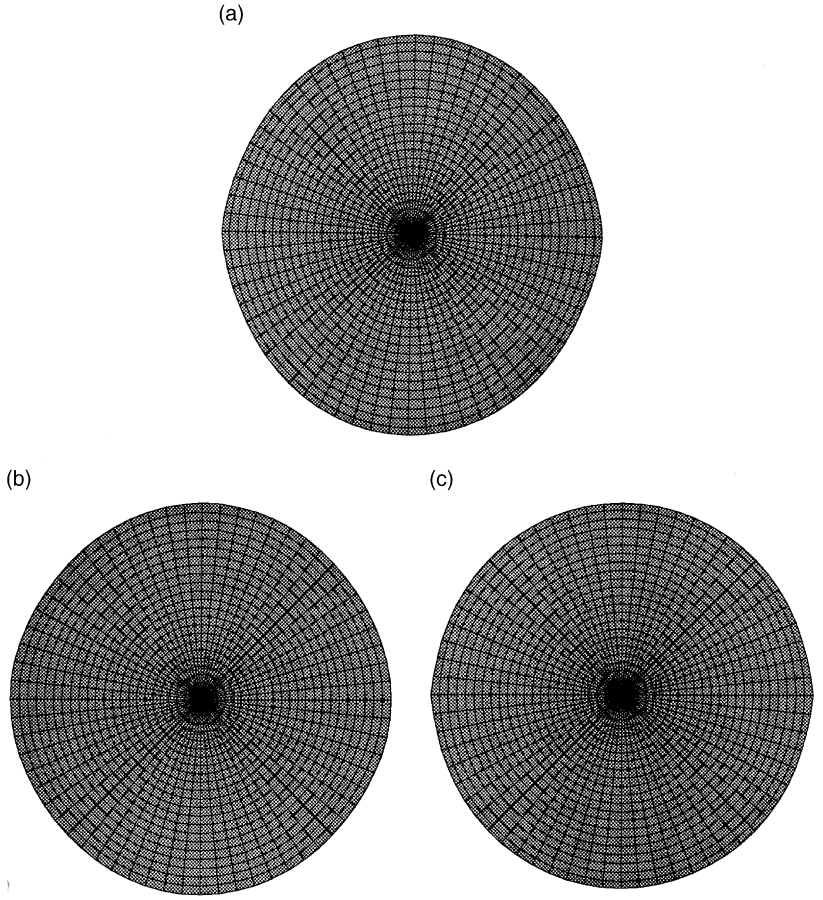

Fig. 19. Exaggerated configurations of an actuator composite paraboloid shell in the second load case ((a) uncontrolled, (b) meridional control and (c) circumferential control).

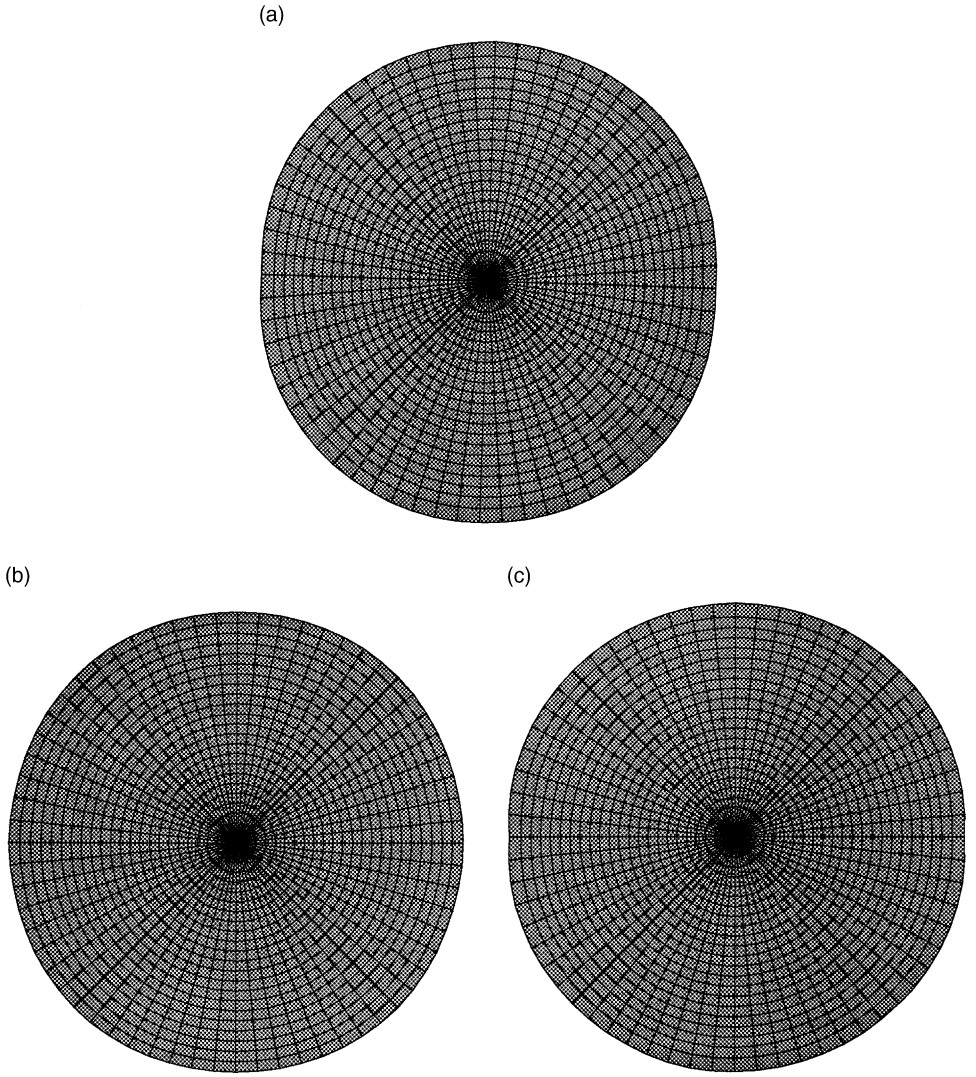

Fig. 20. Exaggerated configurations of an actuator composite paraboloid shell in the third load case ((a) uncontrolled, (b) meridional control and (c) circumferential control).

This is especially true for shape control of a structure against its thermal deformation, because the latter happens all over the structure. This point has been clearly demonstrated in the numerical simulations for thermal deformation control of a paraboloid shell where the thermal deformations on the uncontrolled parts of the shell changed little, whereas those on the controlled parts decreased substantially. For a sensitive structure like a shell of revolution, densely packed actuators are necessary for achieving a better control effect on its thermal deformations. Generally, the convergent behaviour of the control processes illustrated in the applications are satisfactory. A further development of the control algorithm would be a local domain one in which the action of an actuator depends on the sensing measurements of the sensors located in a local domain around it.

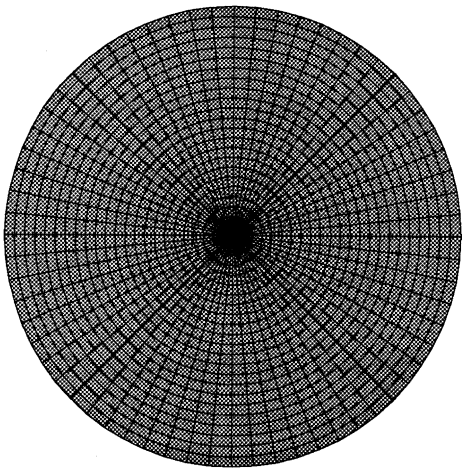

Fig. 21. Original configuration of an actuator composite paraboloid shell.

References

Adeli, H., Saleh, A., 1998. Integrated structural/control optimization of large adaptive smart structures. Int. J. Solids Struct. 35 (28,29), 3815–3910.

Banks, H.T., Smith, R.C., Wang, W., 1996. Smart Material Structures: Modeling, Estimation and Control, Masson/Wiley.

Chandrashekhara, K., Agarwal, A.N., 1993. Active vibration control of laminate composite plates using piezoelectric devices: a finite element approach. J. Intell. Mater. Syst. Struct. 4, 496–508.

Chattopadhyay, A., Seeley, C.E., 1997. A higher order theory for modeling composite laminates with induced strain actuators. Compos. Part B – Engng. 28 (3), 243–252.

Crawly, E.F., Luis, J., 1987. Use of piezoelectric actuators as elements of intelligent structures. AIAA J. 25 (10), 1373–1385.

Crawly, E.F., Lazarus, J., 1991. Induced strain actuation of isotropic and anisotropic plates. AIAA J. 29 (6), 944–951.

Culshaw, B., 1996. Smart Structures and Materials, Artech House.

Gandhi, M.V., Thompson, B.S., 1992. Smart Materials and Structures. Chapman and Hall, London.

Ha, S.K., Keilers, C., Chang, F.K., 1992. Finite element analysis of composite structures containing distributed piezoceramic sensors and actuators. AIAA J. 30 (3), 772–780.

Leissa, A.W., Chang, J.-D., 1996. Elastic deformation of thick, laminated composite shells. Compos. Struct. 35, 153–170.

Lin, C.C., Ko, T.C., 1993. Adhesive interface element for bonding of laminated plates. J. Compos. Struct. 25, 217–225.

Lin, C.C., Hsu, C.Y., Huang, H.N., 1996. Finite element analysis on deflection control of plates with piezoelectric actuators. J. Compos. Struct. 35, 423–433.

Mackerle, J., 1998. Smart materials and structures – a finite element approach: a bibliography 1986–1997. Modell. Simul. Mater. Sci. Engng. 6 (3), 293–334.

Preumont, A., 1997. Vibration Control of Active Structures: An Introduction. Kluwer Academic Publishers, London.

Reddy, J.N., 1984. Exact solution of moderately thick laminated shells. J. Engng. Mech. Div. ASCE 110, 794–805.

Schempp, W., 1982. Complex Contour Integral Representation of Cardinal Spline Functions, American Mathematical Society.